measurements are to be performed and provides a useful research tool for the study of muscle metabolism.

ACKNOWLEDGMENTS

This work was supported by grants from the Finnish Culture Foundation (UR), the Sigrid Juselius Foundation (HI and UR) and the Research and Science Foundation of Farmos (MR). We thank the personnel of the Turku PET Center for their cooperation and Kai Niemi for computer programming assistance.

REFERENCES

1. Elia M. The inter-organ flux of substrates in fed and fasted man, as indicated by arterio-venous balance studies. *Nutr Res Rev* 1991;4:3–31.
2. Laakso M, Edelman SV, Brechtel G, Baron AD. Decreased effect of insulin to stimulate skeletal muscle blood flow in obese man. *J Clin Invest* 1990;85:1844–1852.
3. Jackson RA, Peters N, Advani U. Forearm glucose uptake during the oral glucose tolerance test in normal subject. *Diabetes* 1973;22:442–458.
4. Rabinowitz D, Zierler KL. Forearm metabolism in obesity and its response to intra-arterial insulin. Characterization of insulin resistance and evidence for hyperinsulinism. *J Clin Invest* 1962;41:2173–2181.
5. Elia M, Kurpad A. What is the blood flow to resting human muscle? *Clin Sci* 1993;84:559–563.
6. Lassen NA, Lindberg J, Munck O. Measurement of blood flow through skeletal muscle by intramuscular injection of xenon-133. *Lancet* 1964;i:686–689.
7. Frackowiak RSJ, Lenzi G-L, Jones T, Heather JD. Quantitative measurement of regional cerebral blood flow and oxygen metabolism in man using ^{15}O and positron emission tomography: theory, procedure and normal values. *J Comput Assist Tomogr* 1980;4:727–736.
8. Huang S-C, Carson RE, Hoffman EJ, et al. Quantitative measurement of local cerebral blood flow in humans by positron computed tomography and ^{15}O-water. *J Cereb Blood Flow Metab* 1983;3:141–153.
9. Iida H, Kanno I, Takahashi A, et al. Measurement of absolute myocardial blood flow with $H_2{}^{15}O$ and dynamic positron emission tomography. Strategy for quantification in relation to the partial-volume effect. *Circulation* 1988;78:104–115.
10. Bergmann SR, Herrero P, Markham J, Weinheimer CJ, Walsh MN. Noninvasive quantitation of myocardial blood flow in human subjects with oxygen-15-labeled water and positron emission tomography. *J Am Coll Cardiol* 1989;14:639–652.
11. Iida H, Takahashi A, Tamura Y, Ono Y, Lammertsma A. Myocardial blood flow: Comparison of oxygen-15-water bolus injection, slow infusion and oxygen-15-carbon dioxide slow inhalation. *J Nucl Med* 1995;36:78–85.
12. Kety SS, Schmidt CF. The determination of cerebral blood flow in man by the use of nitrous oxide in low concentrations. *Am J Physiol* 1945;143:53–66.
13. Iida H, Kanno I, Miura S, Murakami M, Kazuhiro T, Uemura K. Error analysis of a quantitative cerebral blood flow measurement using $H_2{}^{15}O$ autoradiography and positron emission tomography with respect to the dispersion of the input function. *J Cereb Blood Flow Metab* 1986;6:536–545.
14. Howard BE, Ginsberg MD, Hassel WR, Lockwood AH, Freed P. On the uniqueness of cerebral blood flow measured by the in vivo autoradiographic strategy and positron emission tomography. *J Cereb Blood Flow Metab* 1983;2:99–108.
15. Snyder WS, Cook MJ, Nasset ES, Karhausen LR, Howells GP, Tipton IH, eds. In: *Report of the task group on reference man*, 1st ed. London: Pergamon Press; 1975.
16. Berne RM, Levy MN, eds. In: *Physiology*, 2nd ed. St. Louis: CV Mosby; 1988.
17. Raitakari M, Knuuti MJ, Ruotsalainen U, et al. Insulin increases blood volume in human skeletal muscle. *Am J Physiol* 1995;269:E1000–E1005.
18. Bailey DL, Jones T, Spinks TJ. A method for measuring the absolute sensitivity of positron emission tomographic scanners. *Eur J Nucl Med* 1991;18:374–379.
19. Iida H, Kanno I, Miura S. Rapid measurement of cerebral blood flow with positron emission tomography. In: *Exploring brain functional anatomy with positron tomography*. Chichester: Wiley; 1991:23–42.
20. Crouzel C, Clark J, Brihaye C, et al. Radiochemistry automation for PET. In: Stocklin G, Pike V, eds. *Radiopharmaceuticals for positron emission tomography*. Dordrecht, Netherlands: Kluwer Academic Publishers; 1993: 54–90.
21. Sipilä HT, Heselius S-J, Saarni HK, Ahlfors T. A compact low-voltage ionization chamber for monitoring positron- and photon-emitters in flowing gases. *Nucl Ins Meth Phys Res* 1985;A238:542–545.
22. Spinks TJ, Jones T, Gilardi MC, Heather JD. Physical performance of the latest generation of commercial positron scanner. *IEEE Trans Nucl Sci* 1988;35:721–725.
23. Smith T, Tong C, Lammertsma AA, et al. Dosimetry of intravenously administered oxygen-15-labeled water in man: a model based on experimental human data from 21 subjects. *Eur J Nucl Med* 1994;21:1126–1134.
24. Nuutila P, Raitakari M, Laine H, et al. Role of blood flow in regulating insulin-stimulated glucose uptake in humans. Studies using bradykinin, [^{15}O]water and [^{18}F]fluorodeoxyglucose and PET. *J Clin Invest* 1996;97:1741–1747.
25. Ebeling P, Bourey R, Koranyi L, et al. Mechanism of enhanced insulin sensitivity in athletes. *J Clin Invest* 1993;92:1623–1631.
26. Meyer E, Yamamoto YL. The requirement for constant arterial radioactivity in the $C^{15}O_2$ steady-state blood-flow model. *J Nucl Med* 1984;25:455–460.

Clinical Fusion of Three-Dimensional Images Using Bremsstrahlung SPECT and CT

E. Ishmael Parsai, Komanduri M. Ayyangar, Ralph R. Dobelbower and Jeffry A. Siegel

Department of Radiation Therapy, Medical College of Ohio, Toledo, Ohio; and Department of Radiation Oncology, Cooper Hospital/University Medical Center, Camden, New Jersey

Infusional brachytherapy for treatment of neoplasms, with colloidal ^{32}P has been used to treat various tumors in the pancreas, liver, brain, lung, and head and neck. In performing such treatments, anatomical verification of the location of the administered ^{32}P from the image obtained by Bremsstrahlung SPECT alone is not possible due to the lack of internal landmarks, since the radionuclide is distributed only in the tumor and does not usually accumulate in the normal organs. The purpose of this study was to provide a practical three-dimensional approach for image fusion between Bremsstrahlung SPECT and CT. **Methods:** The tumors in four cancer patients were injected directly with ^{32}P under CT guidance. A Bremsstrahlung SPECT study using ^{99m}Tc backscatter sources to obtain the body contour was then performed. SPECT images were used to generate the skin contours using a threshold detection method. A three-dimensional surface was generated from these contours using a tiling program and fused with a corresponding CT surface generated from a CT scan in the same patient through an iterative surface-fitting algorithm. The three-dimensional surface of the region of high-activity, corresponding to the infused tumor, was then generated using the Bremsstrahlung SPECT data by mapping the iso-count surfaces through a computer program. The three-dimensional image of the organ then was fused with the registered CT-SPECT datasets. **Results:** The accuracy of fit measured as the mean distance between the SPECT and CT surfaces was in the range of 3–4 mm. **Conclusion:** The anatomical co-registration of Bremsstrahlung SPECT with CT images using the outer surface-fitting algorithm is a reliable tool. This correlation permits direct anatomic confirmation of the region of the ^{32}P activity distribution with the anatomic site selected for injection.

Key Words: Bremsstrahlung; SPECT; phosphorus-32; image fusion; radionuclide therapy

J Nucl Med 1997; 38:319–324

SPECT and CT are well-established diagnostic imaging modalities. These modalities provide complementary information, i.e., SPECT provides functional information whereas CT mainly demonstrates morphology. The fusion of SPECT and CT can increase the information provided by either modality

Received Sept. 20, 1995; revision accepted Mar. 6, 1996.

For correspondence or reprints contact: Komanduri M. Ayyangar, PhD, Professor and Chief of Physics, Medical College of Ohio, Department of Radiation Therapy 3000 Arlington Ave., P.O. Box 10008, Toledo, OH 43699-0008.

alone by providing precise anatomical functional correlation (*1,2*).

In recent years, infusional brachytherapy (*3*) has been used as a new modality for treatment of neoplasms, using colloidal ^{32}P, for treatment of various tumors in the pancreas, liver, brain, lung, and head and neck. The tumor is injected directly with ^{32}P under CT guidance and a Bremsstrahlung SPECT study (*4*) using ^{99m}Tc backscatter sources to obtain the body contour is then performed. This modality allows delivery of extremely high doses of radiation to the tumor while sparing the surrounding normal tissue. The tumor absorbed dose is dependent upon the volume of distribution of ^{32}P, e.g., a 30 mCi (1110 MBq) injection distributed in a 30-cc volume will result in a dose of approximately 7300 Gy. Since the ^{32}P is confined to the tumor region in most cases, the Bremsstrahlung SPECT images usually lack anatomic landmarks and it is not possible to accurately identify the organ in which the ^{32}P accumulation is localized. To improve the clinical efficacy of radionuclide therapy and Bremsstrahlung imaging, it is desirable to use the technique of image fusion between SPECT and CT. This technique allows correlation of areas of increased accumulation of radionuclide on SPECT with specific anatomic structures from the CT study in the same patient.

Image fusion has already been shown to be useful for identifying anatomic sites of radiolabeled antibody accumulation, allowing the accurate staging of tumors before surgery or after treatment (*5–7*). Image fusion between SPECT and CT has also been performed in complicated inflammatory disease (*8*) and for metastatic thyroid carcinoma (*9*). Sgouros et al. (*10*) performed three-dimensional dosimetry for radioimmunotherapy treatment planning using fusion of images from PET with CT and MRI.

Several technical approaches have been used to precisely localize regions of increased activity accumulation on SPECT on the corresponding fused anatomic images of CT (*11*), but to date, no universal method exists. These approaches are based either on internal landmarks or external landmarks (points or lines) which can be identified in both of the volumes to be matched. If region identification is not possible from both these modalities, there is a need for casts and/or fiducial marking systems for both CT and SPECT. This has made many of the current techniques impractical and time-consuming.

Other methods use anatomical contours (*12–14*). A set of transverse slices at approximately the same location in three-dimensional space can be obtained from SPECT and CT. However, the slice thickness, slice position and spatial resolution are different and direct comparison of the imaged structures between these modalities is difficult. Three-dimensional surface contours of SPECT images have been generated by manually outlining contours on serial transverse slices around the periphery of organs that contain radioactivity and can be well-visualized, e.g., the liver (*6*). Similar contours are then drawn around CT slices. The three-dimensional surface outline of the SPECT image ("hat") are then fitted to the anatomic CT images ("head") using an algorithm developed by Pelizarri and Chen (*12*) that minimizes the mean squared distance between points on the two surfaces.

After infusional brachytherapy, anatomical verification of the region of ^{32}P high activity is not possible from the images obtained by Bremsstrahlung SPECT. This is due to the lack of internal landmarks, since the radionuclide is distributed only in the tumor and does not usually accumulate in the normal organs. Also, placement of fiducial markers does not provide a clinically practical tool, since their repeated precise placement is difficult and the technique is unsuited for retrospective studies (*12,13*).

The goal of this study was to develop a three-dimensional surface-fitting algorithm to co-register SPECT and CT datasets in cancer patients undergoing infusional brachytherapy through the use of in-house developed software. It was hoped that this method would also facilitate the co-registration of the area of high activity of the source organ through the use of iso-count distributions, calculated from Bremsstrahlung SPECT data, with the corresponding structure determined from CT. For example, the infused area of high activity or tumor visulized by SPECT can be placed in the anatomic host organ as determined from CT.

MATERIALS AND METHODS

SPECT Technique

SPECT imaging was performed using a Siemen's Multispect-2 dual-head gamma camera system fitted with medium-energy, parallel-hole collimators and interfaced to an ICON computer. An energy window setting of 100 keV ± 25% was used since we previously showed how this narrow window setting has optimal resolution characteristics for ^{32}P (*15*). We have also demonstrated that this energy window is useful for detecting Compton-scattered photons from ^{99m}Tc (*4*), since 90° scatter represents an energy of 110 keV and 180° backscatter represents an energy of 90 keV. As we have previously described (*4*), two sources of ^{99m}Tc (3-cc syringes, filled to 0.5 cc) containing 74–185 MBq each were first placed directly on each of the two collimators, i.e., one per collimator, just outside the field of view of the camera. Immediately after the infusion of ^{32}P, the patient underwent a Bremsstrahlung SPECT study in which the data were acquired in a 64 × 64 image matrix for 32 projections over 180° for each camera head (a total of 64 projections over 360°) for 20 sec per projection using the auto contour rotation mode. Raw data were reconstructed by filtered backprojection in the transaxial, sagittal and coronal planes. The reconstructed slices were one-voxel thick (9.6 mm). Patient-body contour was visualized on each reconstructed transaxial slice by detection of the Compton-scattered photons from the two external sources.

Patients

Four patients were included in this study (one had cancer of the pancreas, two had liver metastases and 1 had lung cancer). Clinical Phase I studies were performed in nonresectable pancreatic cancer, nonresectable non-oat-cell lung cancer, advanced head and neck cancer and liver metastases (*15*). The Phase I trial was based on the direct interstitial administration of 2.5 million particles of macroaggregated albumin followed by colloidal ^{32}P chromic phosphate into the tumor-bearing region performed under CT guidance (*1*). All patients understood the nature of the procedure and gave written consent as approved by our Institutional Review Committee.

All patients were treated with colloidal [^{32}P]chromic phosphate injected as follows: into tumors in the pancreas, 26.680 mCi (987 MBq); liver, 9.918 mCi (367 MBq) and 15.075 mCi (558 MBq) and lung, 9.122 mCi (338 MBq). All patients had a CT study with a 8-mm slice thickness the day of their ^{32}P-SPECT study.

Image Fusion

The analysis of image datasets were performed on a DEC™ Alpha AXP UNIX workstation equipped with AVS™ (Advanced Visual System, Digital Equip. Corp., Maynard, MA) software. Three-dimensional surfaces of the outer contours and other structures were made using a fully developed three-dimensional software package for radiation therapy treatment planning (*17*) at the Medical College of Ohio (MCO). This package was integrated to

handle Bremsstrahlung SPECT imaging data directly and construct three-dimensional surfaces. Using the MCO software integrated with AVS, the images can be co-registered and the closeness of the registration can be visually determined as the three-dimensional object images are rotating in real time. Also, the MCO software allows absolute measurements of translational and rotational parameters.

The CT images were first transferred to a UNIX workstation either through a direct Dicom link with the CT unit, an HP tape reader, or through digitization of the hard copy films. Regardless of the transfer technique, the CT images were stored in a 512 × 512 × 16 bit format along with a header of 2048 bytes. The transaxial reconstructed SPECT data were then transferred to the same UNIX workstation through an algorithm written to directly read these data off the nuclear medicine computer system. Each 64 × 64 × 8 transverse slice of the SPECT data was then mapped to a 512 × 512 image to correspond to the CT image and allow a better contour description with more points than is available in the 64 × 64 matrix.

After transfer of the CT and Bremsstrahlung SPECT data into the UNIX environment and the addition of recognizable header information to each slice, the body contours for both modalities were traced. This was accomplished through a contouring program which included an automated adjustment of the pixel mean and window to easily differentiate between the area of fast gradient counts and air or the background counts. The contour coordinates obtained from each image were converted to real dimensions in Cartesian coordinates using the pixel size, reconstructed diameter, and the table position of the slice. Three-dimensional surface outlines of SPECT images ("hat") were then fitted to the anatomical images obtained from CT ("head") using our custom built software. The algorithm developed at MCO for surface-fitting iteratively determines the transformation that links the two surfaces by executing a direct search in transformation space to minimize the mean squared distance between points on the two surfaces. This algorithm uses an Iterative Closest Point (ICP) technique, based on an optimization routine called MINUIT (*18*). The optimization routine has been adapted to adjust and optimize the parameters (*19*) through numerous iterations until the closest distance possible is obtained with the minimum error.

To visualize the area of high radionuclide activity in three-dimensional space, counts were read from each pixel in each transverse slice of the reconstructed SPECT data and a surface of iso-counts was generated through the MCO three-dimensional treatment planning software. The counts were normalized to the maximum value and displayed along with outer geometry files through the AVS software, which allows the display of iso-count surfaces for any chosen iso-count value. This, when superimposed on the reconstructed volume of entire organ from CT, provided an excellent visualization of spatial localization of the region of high activity with respect to the remainder of the normal organ.

To evaluate the accuracy of the co-registration, the AVS software was used. The three-dimensional surfaces of objects (e.g., outer surface, lung, kidney, liver, etc.) obtained from CT were superimposed on the SPECT outer surfaces and source organs, i.e., areas of infused activity, by visual inspection. Then the absolute quantities of the translational distances and rotations (if any) were measured using the MCO-AVS software. To quantify this accuracy, the mean error between the fused surfaces was calculated through a special computer program developed for this purpose. The program draws several ray lines originating from a selected internal focal point in an identified plane. The intersection of the ray lines with the two matched three-dimensional surfaces is then calculated and the distance between these intersections is determined.

RESULTS

In all four patients, the three-dimensional co-registration was performed and the registration accuracy between SPECT and CT was found to be within 3–4 mm for outer body surfaces. An example of the results from the program that was used to quantify the co-registration accuracy of one of the patients is displayed in Table 1. The first column in Table 1 is the number of points, columns 2 and 3 are the x and y coordinates of the CT data, and columns 4 and 5 display the x and y coordinates of the points from the SPECT dataset. The sixth column displays the z coordinates for both sets of points used. The last column shows the calculated mis-registration errors for the differences between the given points for this patient. The mean misregistration error was found to be 3.6 ± 2.5 mm. Any reasonable number of points can be chosen when calculating the accuracy

TABLE 1
Correlation Between CT (xyz) and SPECT (x'y'z') Surfaces

Point no.	x	y	x'	y'	z-z'	Distance (cm)
1	0	12.59	0	12.9	1	0.3
2	2.2	12.46	2.29	12.96	1	0.51
3	8.05	−6.76	8.35	−7	1	0.38
4	5.77	−6.88	6.2	−7.39	1	0.67
5	−13	−4.73	−13.76	−5.01	1	0.82
6	−14.62	−2.58	−15.1	−2.66	1	0.49
7	−15.54	0	−15.57	0	1	0.02
8	−15.87	2.8	−15.45	2.72	1	0.43
9	−14.84	5.4	−14.73	5.36	1	0.12
10	−13.39	7.73	−13.21	7.63	1	0.21
11	−11.22	9.41	−11.18	9.38	1	0.04
12	−9.01	10.74	−9.22	10.99	1	0.32
13	−6.7	11.6	−6.78	11.74	1	0.15
14	−4.42	12.13	−4.49	12.34	1	0.22
15	−2.2	12.47	−2.23	12.65	1	0.19
16	0	12.98	0	13.07	7	0.09
17	2.27	12.85	2.3	13.03	7	0.19
18	4.6	12.63	4.7	12.9	7	0.29
19	6.85	11.87	7.19	12.45	7	0.67
20	−14.79	0	−15.4	0	7	0.62
21	−15.14	2.67	−15.2	2.68	7	0.06
22	−14.62	5.32	−14.49	5.28	7	0.13
23	−13.33	7.7	−13.1	7.56	7	0.27
24	−11.65	9.78	−11.22	9.42	7	0.56
25	−9.62	11.46	−9.08	10.82	7	0.83
26	−7.05	12.22	−6.81	11.79	7	0.49
27	−4.52	12.41	−4.54	12.47	7	0.06
28	−2.21	12.53	−2.29	12.96	7	0.44
29	0	12.49	0	12.57	13	0.08
30	2.17	12.3	2.23	12.64	13	0.35
31	4.36	11.99	4.61	12.66	13	0.71
32	6.69	11.58	7.06	12.23	13	0.75
33	9.06	10.8	9.43	11.24	13	0.58
34	11.23	9.42	11.39	9.56	13	0.21
35	12.86	7.42	13.22	7.63	13	0.42
36	13.67	4.97	14.52	5.28	13	0.9
37	−13.82	0	−14.56	0	13	0.74
38	−14.26	2.52	−14.42	2.54	13	0.16
39	−13.99	5.09	−14.03	5.11	13	0.04
40	−13.18	7.61	−12.66	7.31	13	0.6
41	−11.5	9.65	−11.06	9.28	13	0.58
42	−9.19	10.95	−9.06	10.79	13	0.21
43	−6.84	11.85	−6.76	11.7	13	0.17
44	−4.45	12.23	−4.49	12.33	13	0.11
45	−2.18	12.36	−2.2	12.51	13	0.15

Mean = 0.363, with s.d. = 0.252.

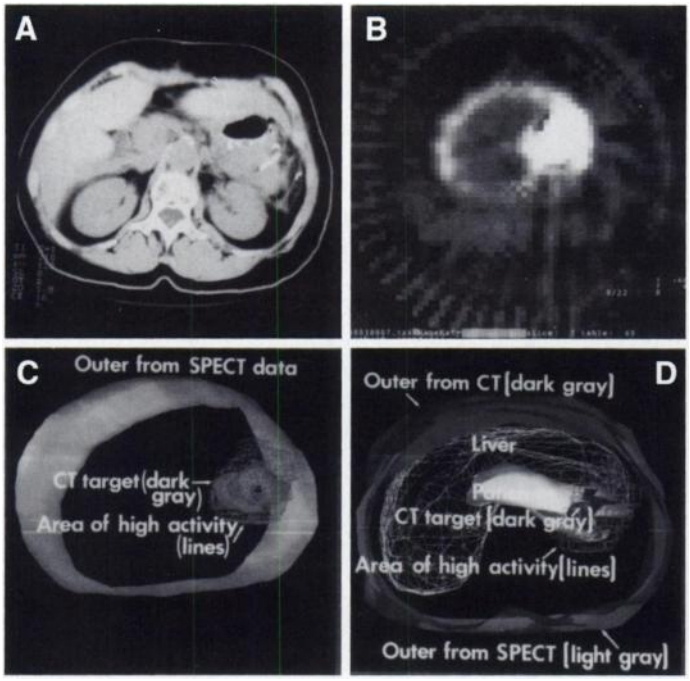

FIGURE 1. (A) CT image of a patient with pancreatic disease shows position of the needle at ^{32}P injection site. (B) SPECT transverse image of the same patient after injection of ^{32}P shows area of high activity. (C) Three-dimensional representation of the patient's outer surface and the iso-count distribution determined from SPECT superimposed with the target from CT. (D) Co-registration of three-dimensional structures.

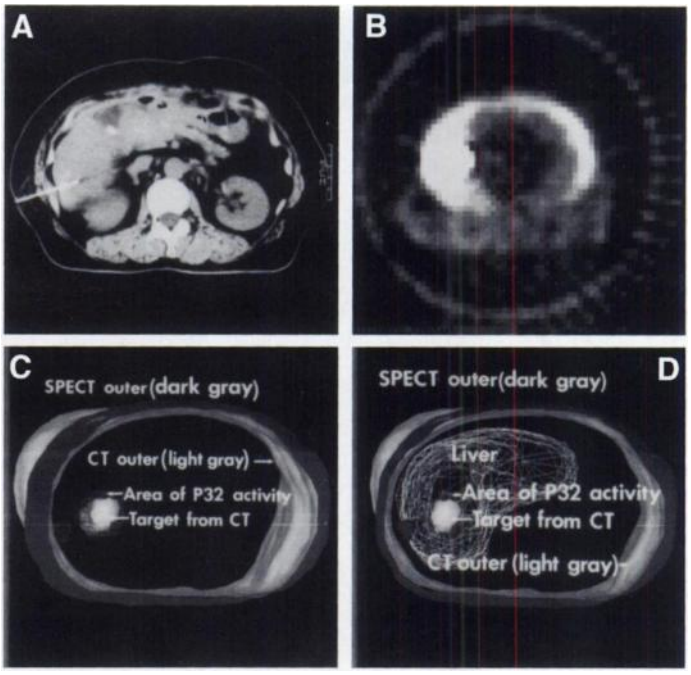

FIGURE 2. (A) Transverse CT image of the abdominal area of a patient with liver disease, where the area of abnormality and the position of needle is shown. (B) SPECT transverse image of the same patient after ^{32}P injection. (C) Three-dimensional co-registration between CT (light gray) and SPECT (dark gray) outer surfaces. The target from the CT slices (solid object) also is shown co-registered with the ^{32}P area of high activity (lines around the target) from SPECT data. (D) Three-dimensional co-registration of all structures. Liver is shown as lines for visibility of target objects.

of the image co-registration; in this case, three contours were selected with 15 points per contour at equal angular intervals resulting in 45 points.

Figure 1A is a transaxial CT slice of a patient with pancreatic cancer showing the infusion needle positioned in the pancreatic tumor. The SPECT transverse image of the same patient is displayed in Figure 2B, which shows the area of high activity. The three-dimensional representation of the body surface generated from Bremsstrahlung SPECT alone and the target (source organ) reconstructed from CT images are shown in Figure 1C. This image also shows the 50% iso-count distributions around the target (shown as lines) generated from mapping the pixel counts that are 50% of the maximum in SPECT images. The co-registration of outer surfaces between Bremsstrahlung SPECT and CT datasets, as well as the fusion of the CT target organ, i.e., the pancreas, with the area of high activity from SPECT, are shown in Figure 1D. The contours of the target area were entered into the computer separately and the target structure reconstructed (solid dark inside the lines) at the tail of the pancreas. When this three-dimensional CT image was superimposed on the SPECT image based on the table position of the contours, it accurately registered on the area of high activity depicted by the Bremsstrahlung SPECT data. Three-dimensional images of the liver and pancreas were also constructed from the CT data and fused in this image.

Figure 2A shows the transverse CT slice of the diseased area of a patient with cancer of the liver, and Figure 2B shows the Bremsstrahlung SPECT transverse image of the same area after injection of the colloidal ^{32}P. The three-dimensional co-registration between CT and SPECT outer surfaces (light and dark gray, respectively) and targets (solid and lines, respectively) is shown in Figure 2C, and the co-registration showing the liver surface (gray lines) and all other structures is shown in Figure 2D.

Figure 3, illustrates: a transverse CT slice of a patient with lung cancer, which shows the area of the abnormality and the position of the needle where colloidal ^{32}P was injected intratumorally (A), the two-dimensional transverse SPECT slice of the same area (B), and the co-registration of the outer surfaces and targets obtained from the CT and SPECT datasets (C).

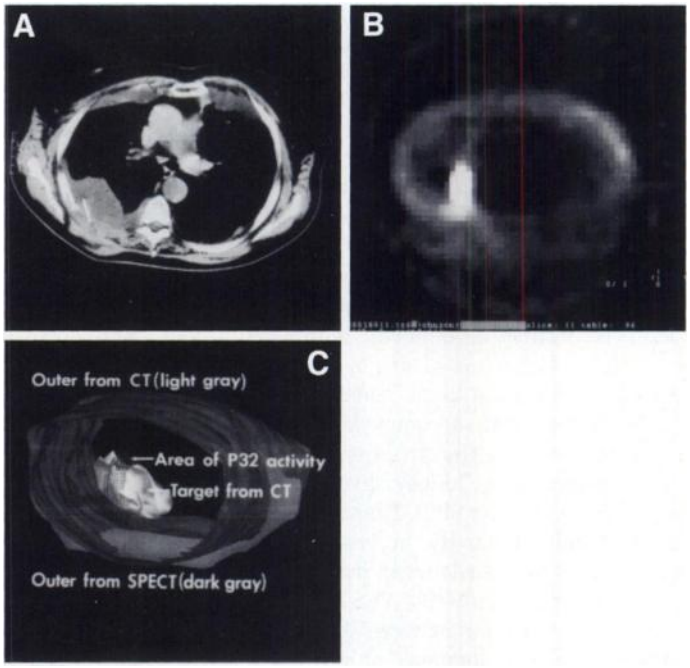

FIGURE 3. (A) Transverse CT image of a patient with lung disease shows the area of abnormality and the position of the needle. (B) SPECT transverse image of the same patient after ^{32}P injection shows the area of high activity. (C) Three-dimensional co-registration between CT (light gray) and SPECT (dark gray) outer surfaces. The target from the CT slices (solid) also is shown co-registered with the ^{32}P area of high activity (lines) from SPECT data.

DISCUSSION

This study demonstrates the feasibility of obtaining accurate fusion images between Bremsstrahlung SPECT and CT scans. The three-dimensional fused images are useful for defining the anatomic location of the selectively injected ^{32}P. Body contour was determined in the reconstructed SPECT transverse slices using two externally placed ^{99m}Tc Compton backscatter sources and commercially available reconstruction software. The body outline definition has been shown to be accurate in patient and phantom studies (*20*). The co-registration methodology used in this study was previously tested using a Jaczszak phantom with simulated lesions (*16*). Tumor simulation was achieved by filling a 38-mm sphere with 150 μCi [^{99m}Tc]pertechnetate. Four external markers containing 50 μCi each of [^{99m}Tc]pertechnetate in small capsules were placed on the phantom and a SPECT study was performed. The same phantom was used for CT imaging after it was cleansed of radioactivity and filled with water. The 38-mm sphere was filled with contrast material and the same size external markers filled with lead were placed on the same locations of the phantom as in the SPECT study. The reconstructed images from both datasets were then co-registered and the visual adequacy of fit was determined.

This approach, when applied to patient data, demonstrated an average alignment accuracy to within 3–4 mm. In view of the relatively poor resolution of SPECT compared to images from other diagnostic imaging modalities such as CT or MR, this result is within acceptable limits for validation of this technique. Other authors using surface-fitting image correlation techniques have reported co-registration accuracies of 3 mm and 2° between phantom and patient datasets for PET studies (*24*), and 1.38 ± 0.65 mm for CT/PET and 2.48 ± 1.09 mm for MRI/PET (*12*) datasets. In patients treated with ^{131}I monoclonal antibody, a co-registration fit within 2 mm with the root mean square distance (RMSD) of 7.4 mm has been reported for CT-SPECT fusion using fiduciary markers (*7*).

The methods previously used for the fusion of SPECT and CT images are varied and have involved the use of external fiduciary markers (*15*), internal anatomic landmarks (*6*) or anatomical contours (*12,14*). These usually result in less accuracy compared to the use of head-holding devices (*22*) and stereotactic methods (*21*) that have been used for the brain.

The use of three-dimensional surface-matching algorithms involves normal tissue uptake for dataset matching (*6*). The use of multiple organs would be better than a single region, but radionuclide uptake in multiple organs may not be present. In any event, the surface-matching approaches cannot be implemented when radionuclides are administered that do not distribute in organs which can be used for surface matching. Scott et al. (*9*) reported a technique using an external fiduciary band that enabled generation of three-dimensional surface contours of the SPECT study by outlining body surface contours on serial transverse slices defined by the band. The use of this fiduciary band is, however, cumbersome. Our method obtains the body contour from SPECT in a much simpler fashion, since the radioactive source is placed on the collimator rather than on the patient's skin. Due to the backscatter source-generated body contour on SPECT, it is possible to adequately perform outer surface matching without the need for internal organ matching.

The approach taken in the present study using the three-dimensional technique for image fusion has many advantages. In general, when delivering any therapeutic dose of radiation to malignant tissue, one obvious concern is the delivery of radiation dose to a carefully delineated target volume. With the aid of a current workstation and the ability to obtain accurate cross-sectional information, the radiation oncology goal of achieving high precision in target localization and dose delivery is closer than ever (*23*). In infusional brachytherapy using colloidal ^{32}P, Bremsstrahlung SPECT imaging is used as a tool to quantify tumor uptake and volume. Furthermore, the delivery of dose to the target is critical, since the radiation dose delivered to the tumor by infusional brachytherapy is higher than that delivered via conventional radiation therapy by more than two orders of magnitude. Therefore, it is crucial to know the precise location of the target, i.e., the area of ^{32}P activity accumulation, and the extent of normal tissue involvement which has a profound effect on the overall outcome of the treatment.

The clinical implication of the image fusion technique provides significant additional information compared to CT or SPECT studies alone. Further studies are underway to evaluate the application of dose-volume histograms (DVHs) in quantitative three-dimensional dosimtery of colloidal ^{32}P using Bremsstrahlung SPECT images.

CONCLUSION

The co-registration technique presented in this article allows direct anatomic confirmation of the site of ^{32}P infusion with the anatomic site selected for injection. It is practical, easy to implement in clinics and can be done in a workstation in approximately 30 min from the time that all images are acquired. The computing time using an up-to-date workstation is relatively short and the majority of time is spent verifying the accuracy of the fused images in all three planes. Image fusion using the outer surface-fitting algorithm is a reliable tool with an accuracy of fit between SPECT and CT surfaces of 3–4 mm.

REFERENCES

1. Swayne LC, Kaplan IL. Image fusion in medicine: an overview using the CT-SPECT model. *J Nucl Med Technol* 1989;17:31–35.
2. Loats H. CT and SPECT image registration and fusion for spatial localization of metastatic processes using radiolabeled monoclonals. *J Nucl Med* 1993;34:562–566.
3. Order SE, Siegel JA, Lustig RA, et al. Infusional brachytherapy in the treatment of non-resectable pancreatic cancer: a new radiation modality (preliminary report of the phase I study). *Antibody Immunoconj Radiopharm* 1994;7:11–27.
4. Siegel JA, Zeiger LS, Order SE, Wallner PE. Quantitative Bremsstrahlung SPECT imaging: use for volume, activity and absorbed dose calculations. *Int J Radiat Oncol Biol Phys* 1995;31:953–958.
5. Kramer EL, Noz ME, Sanger JJ, Megibow AJ, Maguire GQ. CT-SPECT fusion to correlate radiolabled monoclonal antibody uptake with abdominal CT findings. *Radiology* 1989;172:861–865.
6. Scott AM, Macapinlac HA, Divgi CR, et al. Clinical validation of SPECT and CT/MRI registration in radiolabled monoclonal antibody studies of colorectal carcinoma. *J Nucl Med* 1994;35:1976–1984.
7. Koral KF, Zasadny KR, Kessles ML, et al. CT-SPECT fusion plus conjugate views for determining dosimetry in iodine-131 monoclonal antibody therapy of lymphoma patients. *J Nucl Med* 1994;35:1714–1720.
8. Swayne LC. Computer-assisted fusion of SPECT and CT images. Evaluation in complicated inflammatory disease. *Invest Radiology* 1992;27:78–83.
9. Scott AM, Macapinlac H, Zhang J, et al. Image registration of SPECT and CT images using an external fiduciary band and three-dimensional surface-fitting in metastatic thyroid cancer. *J Nucl Med* 1995;36:100–103.
10. Sgouros G, Chiu S, Pentlow KS, et al. Three-dimensional dosimetry for radioimmunotherapy treatment planning. *J Nucl Med* 1993;34:1595–1601.
11. Kessler ML, Pitluck S, Petti P, Castro JR. Integration of multimodality imaging data for radiotherapy treatment planning. *Int J Radiat Oncol Biol Phys* 1991;21:1653–1667.
12. Pelizzari CA, Chen GTY, Spelbring DR, Weichselbaum RR, Chen C. Accurate three-dimensional registration of CT, PET and/or MR images of the brain. *J Comput Assist Tomogr* 1989;13:20–26.
13. Pietrzyk U, Herholz D, Fink G, et al. An interactive technique for three-dimensional image registration: validation for PET, SPECT, MRI and CT brain studies. *J Nucl Med* 1994;35:2011–2018.
14. Chen GTY, Pelizzari CA. Image correlation techniques in radiation therapy treatment planning. *Computerized Med Imaging Graphics* 1989;13:235–240.
15. Siegel JA, Whyte-Ellis S, Zeiger LS, Order SE, Wallner PE. Bremsstrahlung SPECT imaging and volume quantitation with ^{32}P. *Antibody Immunoconj Radiopharm* 1994;7:1–10.
16. Zhang JJ, Ayyangar KM, Park CH, Co-registration of anatomic and functional images in brain tumor therapy. *Proceedings of the Second Sino-American Nuclear Medicine Conference* 1991:50–55.
17. Ayyangar KM, Yeung D, Suntharalingam N, Tupchong L, Hagbin M, Mansfield C. Three-dimensional radiation treatment planning system based on stardent supergraphic workstation. Proceedings of 10th international conference on computers in radiation therapy, Lucknow, India 1990. *Med Phys Bull* 1991;16:36–43.

18. James F, Roos M. Minuit. A system for function minimization and analysis of the parameter errors and correlations Compt. *Phys Commun* 1975;10:343–367.
19. Ayyangar KM, Daftari I, Palta J, Suntharalingam N. Optimization of parameters for fitting linear accelerator photon beams using a modified CBEAM model. *Med Phys* 1989;16:896–901.
20. Siegel JA, Khan SH. Body contour determination and validation for Bremsstrahlung SPECT imaging. *J Nucl Med* 1996;37:495–497.
21. Fox PT, Perlmutter JS, Rachle ME. A stereotactic method of anatomic localization for PET. *J Comput Assist Tomogr* 1985;9:141–153.
22. Zhang J, Levesque MF, Wilson CL, et al. Multi-modality imaging of brain structures for stereotactic surgery. *Radiology* 1990;175:435–441.
23. Marks LB, Spencer DP, Sherouse GW, et al. The role of three dimensional functional lung imaging in radiation treatment planning: The functional dose-volume histogram. *Int J Radiat Oncol Biol Phys* 1995;33:65–75.
24. Yu JN, Fahey FH, Harkness BA, Cage HD, Eades CG, Keyes JW. Evaluation of emission transmission registration in thoracic PET. *J Nucl Med* 1994;35:1777–1780.

A "Hybrid" Method for Measuring Myocardial Wall Thickening from Gated PET/SPECT Images

Irène Buvat, Marissa L. Bartlett, Anastasia N. Kitsiou, Vasken Dilsizian and Stephen L. Bacharach
Department of Nuclear Medicine, Cardiology Branch, National Institutes of Health, Bethesda, Maryland; and U66 INSERM/CNRS, Paris, France

We introduce a hybrid index, HYB, which combines counts with geometric information to measure wall thickening from PET/SPECT gated images. Its accuracy is compared with that of a count-based index (MAX) and a geometric index (FWHM). **Methods:** For each index, the index values versus thickness and the estimated thickening values versus true thickening were investigated using theoretical analyses, realistic simulated data obtained from clinical gated MR scans, phantom measurements and preliminary gated MRI and PET patient studies. Each index was studied for different spatial resolutions and noise and background conditions. The performance of each index was quantified using a parameter "Q" reflecting bias and variability of thickening estimates. **Results:** HYB varied more linearly with thickness than MAX and FWHM, resulting in a better Q value than with MAX and FWHM for all noise, background and spatial resolutions. ROC analysis confirmed that HYB significantly increases the sensitivity and specificity for detection of wall thickening abnormalities (sensitivity = 100%; specificity = 85% for HYB, 95% and 50% for MAX and 100% and 0% for FWHM, respectively). **Conclusion:** Use of the hybrid index instead of conventional count-based or geometric indices should improve the classification of normal/abnormal wall thickening values in gated SPECT and PET.

Key Words: myocardial wall thickening; heart; receiver operating characteristic curve

J Nucl Med 1997; 38:324–329

Left ventricular (LV) wall thickening is a valuable indicator of myocardial contractile function. PET and SPECT imaging enable the assessment of myocardial perfusion and metabolism in vivo. With ECG gating, PET and SPECT images may also be used to estimate LV wall thickening, thereby permitting simultaneous measurement of regional function with perfusion or metabolism (*1,2*).

The LV wall thickness is usually less than 20 mm. For a normal subject, typical wall thickening is about 4 mm, from 10 mm at end-diastole to 14 mm at end-systole (*3*). Less than 2 mm thickening is abnormal. To measure such small but clinically important variations, several methods have been proposed, which can be categorized as either count-based or geometry-based. The most common count-based method used in PET (*1,4*) and SPECT (*5–7*) relies on the percent count increase from end-diastole to end-systole as an index of wall thickening. Geometric methods include tracking the endo- and epi-cardial borders (*8*) and model fitting (*9*). Both the count-based and the geometry-based methods have advantages as well as serious limitations.

A theoretical and experimental investigation of the count-based and geometric methods led us to introduce a new hybrid method. This hybrid method combines count information with geometric information in a manner that preserves the best features of both approaches. The hybrid method yields an index that theoretically has a more linear behavior with thickening than indices produced by either the count-based or geometric method alone. The performances of the count-based, geometric and hybrid methods are evaluated using: (a) realistic simulated data obtained from clinical gated MR scans, (b) phantom measurements and (c) preliminary gated MRI and PET patient studies. Results from the MRI-based simulations are reported for different spatial resolutions, noise and background conditions, which cover the most realistic PET and SPECT imaging situations. Preliminary patient data are presented to illustrate the potential clinical benefit of the new hybrid index.

MATERIALS AND METHODS

Data Analysis Scheme

LV regional wall thickening was determined from short-axis gated images after dividing each short-axis image into a number of sectors. First, at each of the "T" gated time points, each short-axis slice was sinc interpolated (*10*) by a factor of four to minimize sampling effects. An initial, manual estimate of the LV center was made on the end-diastole image. Based on this initial position, the optimum center was estimated as that position equidistant from the maxima of all profiles across the myocardium. This optimum center was used to cast the LV short-axis image into cylindrical coordinates. Based on this cylindrical coordinate system, the LV was divided into "S" sectors and a profile (plot of counts as a function of distance from endo- to epi-cardium) was computed. The process was repeated at each time point, using the optimal center point from time point "k-1" as the initial center estimate for the kth time point image. Therefore, for each slice, there were TxS count-profiles. For each sector's profile, an index related to that sector's thickness was then calculated.

Indices for Measuring Wall Thickening

Count-based, geometric and hybrid indices were studied.

Received Oct. 2, 1995; revision accepted Jan. 28, 1996.
For correspondence or reprints contact: Stephen Bacharach, PhD, National Institutes of Health, Department of Nuclear Medicine, Building 10, Room 1C401 , Bethesda, MD 20892.